Chemical Physics Letters 778 (2021) 138812

Contents lists available at ScienceDirect

Chemical Physics Letters

journal homepage: www.elsevier.com/locate/cplett

Rapid melting and revitrification as an approach to microsecond time-resolved cryo-electron microscopy

Jonathan M. Voss, Oliver F. Harder, Pavel K. Olshin, Marcel Drabbels, Ulrich J. Lorenz *

Laboratory of Molecular Nanodynamics, École Polytechnique Fédérale de Lausanne, 1015 Lausanne, Switzerland

ARTICLE INFO

Keywords:
Protein dynamics
Time-resolved cryo-electron microscopy
Single-particle observation
In situ transmission electron microscopy
Graphene liquid cells

ABSTRACT

Proteins typically undergo dynamics on the microsecond to millisecond timescale, which is much faster than the time resolution of cryo-electron microscopy. Here, we propose a novel approach for microsecond time-resolved cryo-electron microscopy that involves melting a cryo specimen *in situ* with a laser beam. The sample remains liquid for the duration of the laser pulse, offering a tunable time window in which the dynamics of embedded particles can be induced in a liquid environment. After the laser pulse, the sample vitrifies, trapping particles in their transient configurations. As a proof of principle, we study the disassembly of particles after they incur structural damage.

1. Introduction

Proteins perform a range of tasks that are quintessential for life. They are involved in harvesting energy, maintaining homeostasis, catalyzing metabolic reactions, reproduction, and sensing stimuli. As nanoscale machines, proteins are dynamic systems whose free energy surface determines their motions and characteristic timescales [1]. Backbone motions and side-chain rotations involve transitions between minima separated by small barriers and typically occur on picosecond to nanosecond timescales, leading to fast, small-amplitude fluctuations of the protein structure [2]. In contrast, the dynamics associated with the activity of a protein frequently involve large-amplitude motions of entire domains that occur on a timescale of microseconds to milliseconds [1,2].

Much of our knowledge about protein function derives from static structures at atomic resolution, which frequently allow one to infer function, particularly if structures of different functional states can be obtained [3–6]. However, in the absence of real-time observations, our understanding of proteins is necessarily incomplete. Directly observing proteins as they perform their tasks, in real time and at atomic resolution, holds the promise of fundamentally advancing our grasp of these nanoscale machines [1].

X-ray crystallography has long been the most important tool in structural biology [7]. Recently, the advent of bright x-ray pulses has also made it possible to carry out time-resolved experiments, even with ultrafast time resolution [8,9]. However, the requirement of a crystalline sample poses a specific challenge for studying the dynamics of proteins, as the crystal packing hinders large-amplitude motions [10–12]. In contrast, single-particle cryo-electron microscopy (cryo-EM) [13–19] enables the observation of biological specimens in their frozen hydrated state [20,21]. The revolution that the field has recently undergone has also created new opportunities for obtaining time-resolved information [22,23]. In time-resolved cryo-EM, dynamics are induced by mixing two reactants [24–26] or exposing the sample to a short light pulse [27,28]. Short-lived intermediates are then trapped in vitreous ice by promptly plunge freezing the sample. However, with a time resolution of several milliseconds [22], which is ultimately limited by the timescales for plunging (~5 ms) [28] and vitrification (~1 ms) [21], this technique is currently too slow to capture many relevant processes.

Here, we propose a novel approach for carrying out time-resolved cryo-EM with microsecond time resolution. The concept (Fig. 1a–e) is based on rapidly melting a vitrified sample *in situ* with a heating laser (Fig. 1a). Once in their native liquid environment at room temperature (Fig. 1b), the embedded particles are subjected to an external stimulus that induces dynamics (Fig. 1c). For example, a second laser pulse can be used to photoactivate a caged compound and liberate ATP or a small peptide that interacts with the protein [29,30]. In the simplest case, the heating laser itself can be used to create a temperature jump to initiate conformational dynamics. At a well-defined point in time, the heating laser is switched off to induce rapid revitrification and trap the particles in their transient configurations (Fig. 1d), so that they can be subsequently characterized with established cryo-EM techniques (Fig. 1e).

It is not obvious that implementing such a scheme should be possible.

* Corresponding author.
E-mail address: ulrich.lorenz@epfl.ch (U.J. Lorenz).

https://doi.org/10.1016/j.cplett.2021.138812
Received 26 March 2021; Received in revised form 21 May 2021; Accepted 3 June 2021
Available online 11 June 2021

Usually, warming up a cryo sample is scrupulously avoided in order to prevent devitrification. Here, we demonstrate that this obstacle can be overcome. We employ cryo samples with a holey gold film [31] supported by a gold mesh. For some experiments, we additionally sandwich the sample between two sheets of few layer graphene, as illustrated in Fig. 1f (Note S1 and Fig. S1), so as to reduce evaporation of the liquid water in the vacuum of the microscope [32]. The sample is heated *in situ* with a laser pulse of tens of microseconds duration (532 nm, 24 μm FWHM spot size), which we obtain by chopping the output of a continuous laser with an acousto-optic modulator [33] (Note S3 and Fig. S2). The gold film and graphene sheets strongly absorb at the laser wavelength and serve as the heat source to melt the ice. In contrast, neither the proteins nor the ice absorb the laser radiation, which prevents photodamage to the specimen. In all experiments, we have centered the heating laser onto the area under observation.

2. Results and discussion

2.1. Rapid in situ melting and vitrification

We first demonstrate that it is indeed possible to melt a cryo sample *in situ* and subsequently achieve rapid vitrification. To this end, we intentionally prepare crystalline ice samples, which allows us to directly verify the success of the experiment. Fig. 2a shows a thin ice sheet held at 100 K that is suspended over a hole of the gold film and enclosed between graphene layers. Bend contours are visible, indicating that the ice sheet is crystalline. This is confirmed by the diffraction pattern, which exhibits the signature of hexagonal ice [21] (Fig. 2b). When we irradiate the sample with an individual 20 μs laser pulse with a power of 25 mW, the diffraction pattern remains largely unchanged (Fig. 2c), indicating that the sample has not melted. Laser pulses of up to 63 mW yield the same result (Fig. 2d–g). However, a single pulse with a power of 75 mW provides sufficient heat to induce melting (Fig. 2h). Most of the ice sheet now exhibits homogeneous contrast, with the diffraction pattern revealing the signature of vitreous ice [21] (Fig. 2i, selected area marked by the green circle in Fig. 2h). In the top left of the sample, a small void has formed. We observe such voids if defects in the graphene sheets allow liquid water to evaporate. The lighter contrast on the right side of the sample indicates an area where some ice has remained crystalline, as a selected area diffraction pattern reveals (Fig. 2i inset, selected area indicated with a grey circle in Fig. 2h). Evidently, at this laser power, the ice sheet barely reaches the melting point and remains partially crystalline. Incrementally increasing the laser power thus provides an *in situ* calibration of the power required for melting.

For the experiment illustrated in Fig. 3a–d, the threshold laser power for melting and vitrification was first calibrated in a different area of the

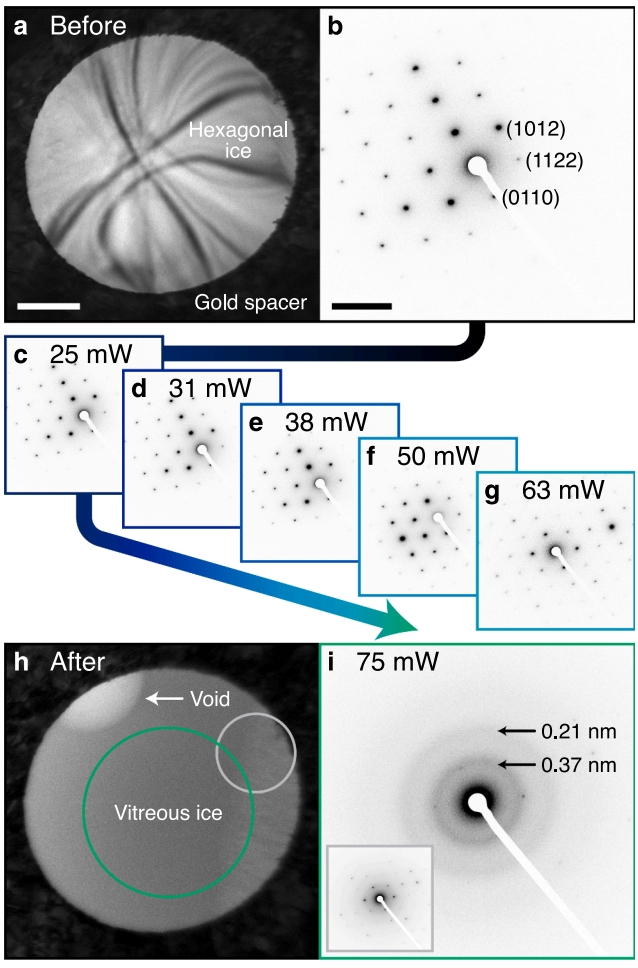

Fig. 2. Determination of the laser power required for *in situ* melting and vitrification. (a) Micrograph and (b) selected area diffraction pattern of a thin film of hexagonal ice. (c–g) The sample is irradiated with individual laser pulses of 20 μs duration. As the laser power is increased up to 63 mW, the diffraction pattern remains largely unchanged, indicating that melting has not occurred. (h,i) A single pulse with a power of 75 mW provides sufficient heat to melt the sample, which then rapidly vitrifies after the end of the laser pulse. Scale bars, 300 nm and 4 nm^{-1}.

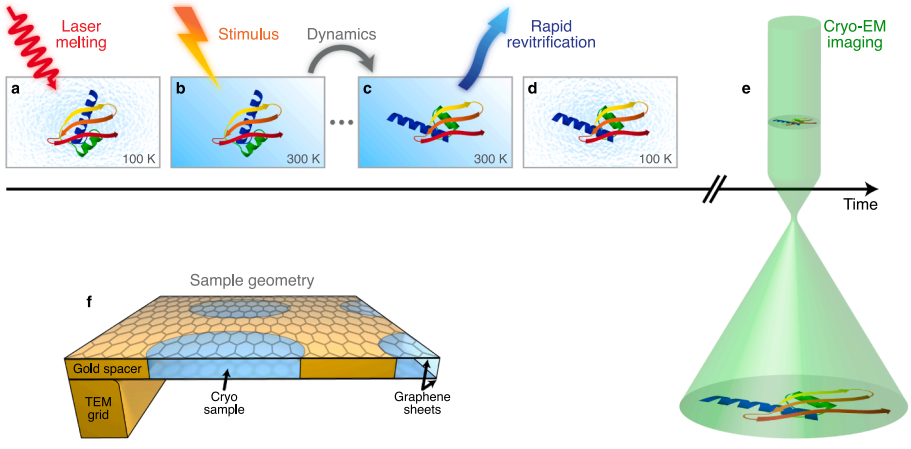

Fig. 1. Experimental concept and sample geometry. (a–e) Illustration of rapid *in situ* melting and revitrification for time-resolved cryo-EM. (a) A cryo sample is melted *in situ* with a heating laser. (b) Once the sample is liquid and has reached room temperature, dynamics of the embedded particles are induced with an external stimulus, *e.g.* a short second laser pulse that releases a caged compound such as ATP or a peptide. (c) While the particle undergoes conformational changes, the heating laser is switched off at a given point in time so that the sample rapidly cools and revitrifies. (d) The particle is trapped in its transient configuration and can be subsequently imaged with conventional cryo-EM techniques (e). (f) Illustration of the sample geometry. A cryo sample supported by a holey gold film is enclosed between two graphene layers, which prevent evaporation in the vacuum of the microscope as the sample is melted *in situ* with a laser pulse.

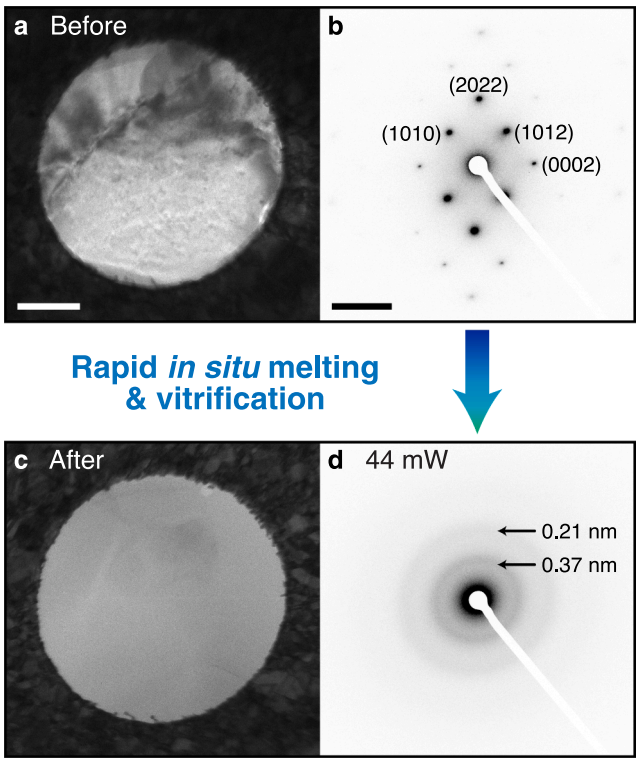

Fig. 3. *In situ* melting and vitrification with a single laser pulse. (a) Micrograph and (b) selected area diffraction pattern of a thin film of hexagonal ice. (c,d) After calibration of the laser power in a different area, the sample is successfully melted and vitrified with a single laser pulse. Scale bars, 300 nm and 4 nm^{-1}.

sample. When we use this power to heat the crystalline sample in Fig. 3a, b, melting and vitrification is achieved with a single laser pulse (Fig. 3c, d). The uniform contrast suggests that here, the ice film suspended across the hole has completely vitrified. We note that the laser power needed to induce melting is lower than in Fig. 2, where the sample is in close proximity to the bars of the TEM grid. Heat transfer simulations agree with this observation, showing that the required power increases closer to the bars (Note S4 and Fig. S3).

2.2. *Characterization of the temperature evolution and time resolution*

For the purpose of time-resolved cryo-EM experiments, it is crucial to have a detailed understanding of the temperature evolution of the sample, which ultimately determines the attainable time resolution. We therefore characterize the heating and cooling dynamics *in situ* with time-resolved electron microscopy [34–38] (Note S5 and Fig. S2). We heat the sample in Fig. 4a, which is held at 100 K, with a 20 μs laser pulse (13 mW). To probe its temperature at a specific point in time, we record a time-resolved diffraction pattern of a selected area of the gold film with a 1 ns electron pulse (~10^4 electrons). The diffraction intensity of the gold film decreases exponentially with temperature (Debye-Waller behavior [39]) and therefore provides a suitable probe of the sample temperature. We then repeat the experiment stroboscopically (1 kHz repetition rate) to probe the temperature at different points in time. Since a thin layer of ice would not be stable under illumination with thousands of laser pulses, we perform the experiment in the area shown in Fig. 4a, which is not covered by ice. Nevertheless, the temperature evolution of the bare gold film provides a good approximation of the heating and cooling dynamics of a cryo sample. As discussed in detail below, simulations confirm that the presence of a thin ice film barely alters the temperature evolution. Moreover, the ice and the underlying gold film have near-identical temperatures.

Fig. 4b shows a diffraction pattern of the holey gold film collected from the area marked with a red dot in Fig. 4a, onto which we have also aligned the heating laser. As the laser warms the sample, the diffraction intensity decreases quickly, as shown for the (3 3 1), (4 2 0), and (4 2 2) reflections in Fig. 4c. After only a few microseconds, the temperature in the selected area stabilizes, increasing only slightly over time. When the heating laser is switched off at 20 μs, the sample promptly recools as it dissipates heat towards its surroundings, which have remained at cryogenic temperature. From exponential fits (solid red curve, Note S6,7), we obtain heating and cooling times of 1.2 μs and 3.6 μs, respectively. Similar timescales are obtained in different areas of the sample (orange and yellow dots in Fig. 4a and Fig. S4e,f).

Heat transfer simulations (Note S4 and Fig. S3) reproduce these timescales reasonably well, yielding 1.0 μs heating and cooling times (Fig. 4d, solid red curve). If we add a thin layer of vitreous ice, its temperature (blue curves) closely follows that of the underlying gold film, with which it is in close contact. With increasing ice thickness, the heating and cooling times become longer. However, the temperature at which the sample stabilizes during the laser pulse barely changes. We find that the sample temperature plateaus at 300 K for a laser power of 35 mW (Fig. 4d), which is in reasonable agreement with the experimentally determined power that induces melting.

It may appear counterintuitive that melting a cryo sample *in situ* should result in vitrification, since heating up a vitreous sample ordinarily causes irreversible crystallization [40]. The characterization of the temperature evolution reveals that this is made possible by the high heating and cooling rates of nearly 10^8 K/s, which is more than two orders of magnitude faster than what is required to outrun crystallization and achieve vitrification [41,42]. Several factors enable such fast cooling. The tightly focused laser beam heats the sample only locally, so that after the laser pulse, the heat can be rapidly dissipated to adjacent areas that have remained at cryogenic temperature. Our simulations also reveal that the bars of the specimen grid play an important role in this respect. Due to their large heat capacity, they barely warm up and therefore act as an effective heat sink. Crucially, the cooling rate also determines how fast the dynamics of embedded particles can be arrested, which occurs when the sample is cooled below the glass transition temperature of water at 137 K [43,44]. We conclude that for ice thicknesses suitable for cryo-EM, our approach yields a time resolution of 5 μs or better, three orders of magnitude faster than what is currently possible with time-resolved cryo-EM [22]. Importantly, this matches the time resolution of cryo-EM to the characteristic timescale on which the relevant dynamics of most proteins occur [1,2]. Snapshots of the dynamics at different points in time can then be acquired by simply changing the duration of the heating laser pulse.

2.3. *Proof of principle experiment*

As a proof of principle, we study the rapid disassembly of the GroEL protein complex [45] in response to structural damage that we induce through electron beam irradiation. It is well-known that proteins are heavily damaged during cryo-imaging with typical electron doses [46,47]. However, the cryogenic matrix traps fragments in place and thus limits structural degradation, which would otherwise render high-resolution imaging impossible [46,47]. In a liquid environment, however, structural changes can freely occur. Melting a cryo sample *in situ* after it has been exposed to a significant electron dose should therefore allow the damaged proteins to unravel.

Fig. 5a shows a cryo sample of GroEL on a holey gold film, imaged with a dose of 14 electrons/$Å^2$. Here, we have illuminated only the top part, so that particles in the unexposed area do not incur any beam damage and can serve as a control. For simplicity, the sample is not enclosed between graphene sheets. Even though this allows some water to evaporate during laser heating, it is still possible to carry out experiments with laser pulse durations of tens of microseconds without evaporating the entire sample. In order to allow dynamics of the beam-

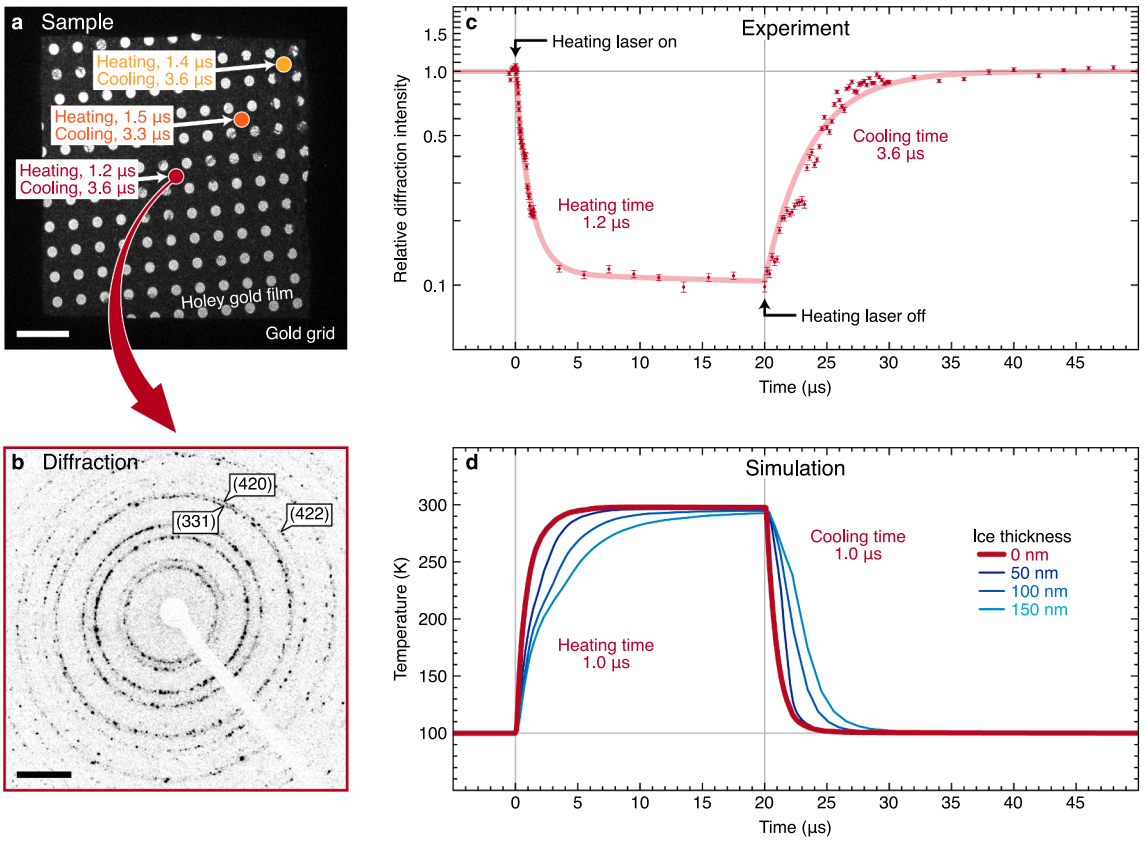

Fig. 4. Characterization of the temperature evolution of the sample under illumination with microsecond laser pulses. (a) Micrograph of the sample in an area that is free of ice. Heating and cooling timescales of the gold film were measured at three different positions (dots), onto which the laser was focused. Scale bar, 5 µm. (b) Selected area diffraction pattern of the area marked with a red dot in (a). Scale bar, 5 nm^{-1}. (c) Temporal evolution of the intensity of the (3 3 1), (4 2 0), and (4 2 2) reflections in (b) under irradiation with a 20 µs laser pulse (dots). Heating and cooling times of 1.2 µs and 3.6 µs, respectively, are determined from fits with exponential functions (solid curve). The error bars represent the standard error. (d) A simulation of the temperature evolution of the sample in (c) yields similar heating and cooling times of 1.0 µs (solid red curve). In the presence of a layer of vitreous ice (blue curves), heating and cooling times increase, while the maximum temperature at which the sample stabilizes barely changes.

damaged GroEL to occur, we melt the sample with a 10 µs laser pulse, after which it revitrifies, arresting the particles in their transient configurations (Fig. 5b). The irradiated area (dashed line) appears lighter than the remainder of the sample, a phenomenon that we consistently observe, but that is absent without electron beam exposure. This suggests that this area has thinned as volatile radiolysis products trapped in the ice [47] were liberated during the melting process (see also Fig. S5). The proteins are no longer visible in this area, indicating that they have disintegrated, leaving only fragments that offer little contrast. A few larger fragments are visible near the edge of the irradiated area (red arrows). The proteins in the bottom part of the image, which had not been exposed to the electron beam, have remained intact. This demonstrates that the disintegration of GroEL particles we observe is caused by electron beam irradiation and not the melting and revitrification process.

The effect of exposure to the electron beam appears to extend beyond the irradiated area. In its immediate vicinity, the particle density is lower, and partially disassembled proteins as well as fragments are visible (red arrows). A possible explanation is that melting liberates highly reactive radiolysis products trapped in the ice, such as OH and H radicals, protons, and solvated electrons [47]. The diffusion lengths of these species within the laser pulse duration of 10 µs are hundreds of nanometers [48], suggesting that they will reach intact GroEL particles and damage them. It is also possible that convective flow of the water film occurs as areas of different thickness equilibrate. With increasing duration of the heating laser pulse, convection seems to play a larger role since the spatial distributions of intact particles and fragments are increasingly reshuffled, as shown for a 30 µs laser pulse in Fig. S5. After irradiation with a 50 µs laser pulse (Fig. 5c,d), the ice thickness is almost homogeneous across the hole in the gold film, with intact particles and fragments visible in both the exposed and unexposed areas (Fig. 5d, insets).

We note that the disintegration of the proteins observed in Fig. 5d does not result from the laser irradiation, but is only present if the sample has first been exposed to the electron beam. This is evidenced by Fig. S6, which shows a neighboring hole of the gold film that had not been irradiated by the electron beam. The particles in this hole are intact, even though they were exposed to a near-identical laser intensity and reached a similar temperature (the FWHM of the Gaussian laser spot, which is centered on the sample, is more than an order of magnitude larger than the distance separating the holes).

Lowering the electron dose reduces the damage inflicted on the GroEL particles, so that their disintegration proceeds more slowly, allowing us to take snapshots of different stages. If we irradiate the sample with only 1.4 electrons/$Å^2$ (Fig. S7), the particles do not disintegrate entirely when the sample is melted with a 10 µs laser pulse (Fig. 5e). Instead, a large number of damaged proteins and fragments remain visible in the exposed area. Increasing the laser pulse duration to 20 µs allows the disassembly to proceed further (Fig. 5f). Few particles remain that resemble intact GroEL, while the size of the fragments has further decreased. We note that we have adjusted the laser power with the procedure described in Fig. 2, so that we can be certain that the plateau temperature of the sample exceeds the melting point of ice. Moreover, heat transfer simulations show that for the particular sample

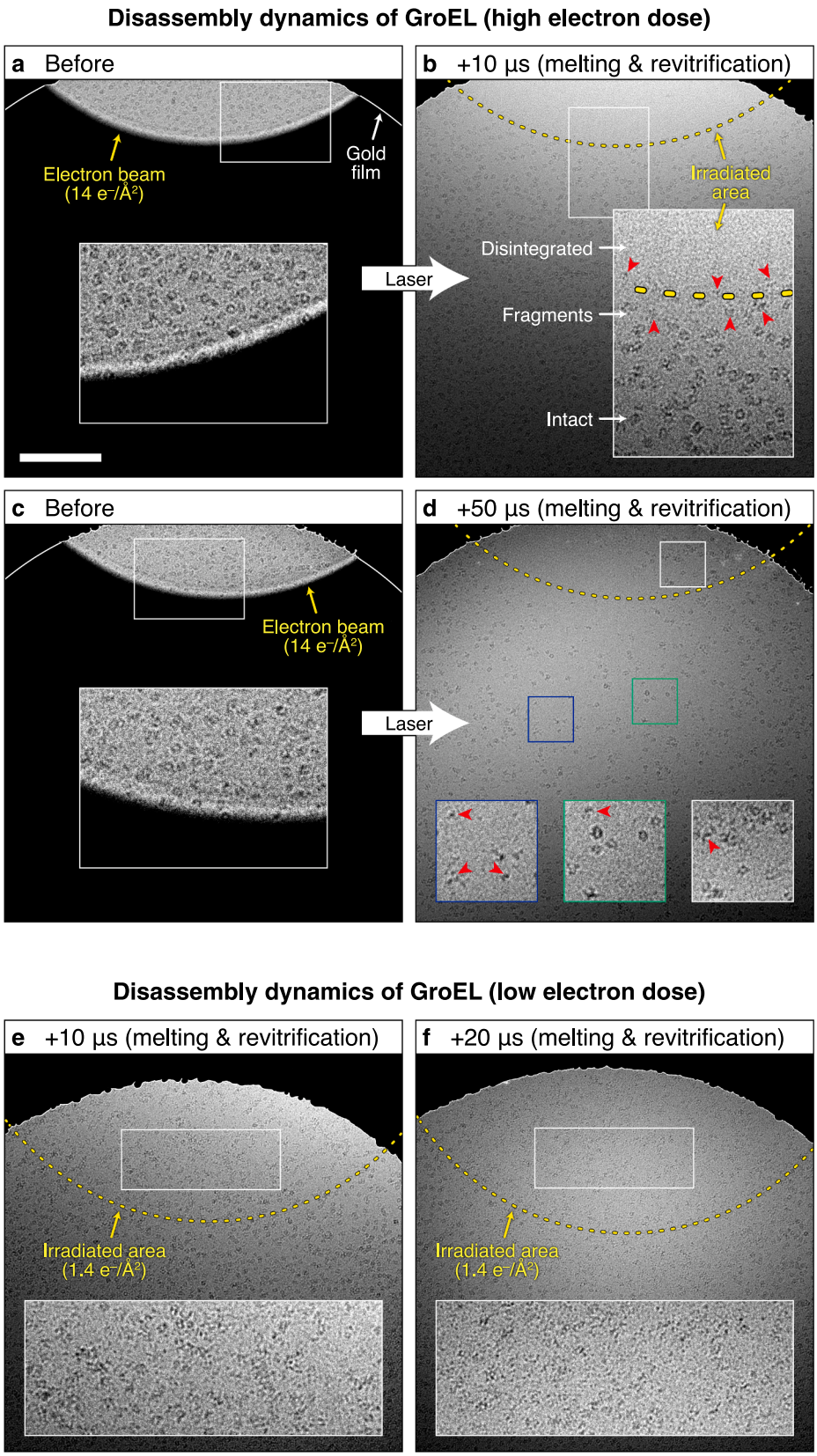

Fig. 5. Microsecond time-resolved cryo-EM of the rapid disassembly of GroEL following electron beam damage. (a) Micrograph of GroEL on a holey gold film. Only the top part is illuminated with the electron beam (14 electrons/Å^2) in order to limit beam damage to particles in that area. The lines sketch the outline of the hole of the gold film. (b) The sample is melted with a 10 µs laser pulse *in situ*, allowing the damaged GroEL particles to unravel. After the laser pulse, the sample revitrifies, trapping particles in their transient configurations. The dashed line delineates the sample area that was irradiated in (a). The red arrows highlight protein fragments that are visible at the boundary of the irradiated area. (c,d) The experiment in (a,b) is repeated with a 50 µs laser pulse. (e,f) The electron beam damage inflicted on the GroEL particles is reduced by lowering the electron dose to 1.4 electrons/Å^2. Melting the sample with a laser pulse of 10 µs (e) and 20 µs duration (f) traps the particles in different stages of the disassembly process. In the insets, the contrast has been adjusted to make the particles more easily visible. Scale bar, 250 nm.

geometry used here, evaporative cooling limits the plateau temperature, so that it should not exceed room temperature for the laser powers employed (Fig. S8).

3. Conclusions and outlook

We have demonstrated that it is possible to rapidly laser melt and revitrify a cryo sample *in situ*, so that particle dynamics can occur in

liquid for a well-defined amount of time. This opens up the perspective of carrying out microsecond time-resolved cryo-EM experiments. In a proof of principle experiment, we have observed the disassembly of GroEL following electron beam damage, which reveals a surprising insight about cryo-imaging. Even at a dose as low as 1.4 electrons/Å^2, damage to the particles is so extensive that once the vitreous ice matrix that preserves their shape is melted, they completely disintegrate. These initial results suggest that our method may be applicable to a wider range of processes. For instance, it is straightforward to implement temperature jump experiments by adjusting the laser power to heat the sample well above room temperature, which should make it possible to study folding and unfolding dynamics. Another possibility is to trigger dynamics with an additional laser pulse once the sample reaches room temperature. In the case of a photoactive protein [8,49], the laser pulse itself can initiate the dynamics. Alternatively, it can provide a biomimetic trigger by dissociating a photo-activated caged compound to release ions, ATP, or small peptides, or to induce a pH jump [29,30,50]. Such experiments could be simplified by activating the photorelease compounds already in the vitreous state of the sample. Since the proteins are unable to undergo dynamics in the vitreous ice matrix, the trigger can only become active once the sample is melted. We have in fact demonstrated such a scheme in the experiments of Fig. 5, where the trigger, electron beam irradiation, was applied before *in situ* melting. Precise control of the sample temperature will be crucial for such experiments to succeed. The laser power needed to reach a given sample temperature can be calibrated *in situ* by determining the threshold power for melting (Fig. 2). Fortunately, small variations in the thickness of the ice layer do not change the plateau temperature of the sample (Fig. 4d). This is particularly true for samples not enclosed in graphene, for which evaporative cooling stabilizes the temperature.

Declaration of Competing Interest

The authors declare that they have no known competing financial interests or personal relationships that could have appeared to influence the work reported in this paper.

Acknowledgements

The authors acknowledge Christoph Schillai for his input on sample preparation and for critically reading the manuscript. We kindly thank the Centre Interdisciplinaire de Microscopie Electronique and the Plateforme Technologique de la Production et Structure des Protéines at EPFL for use of equipment. We thank D. Demurtas and K. Lau for their support and helpful discussions. This work was supported by the ERC Starting Grant 759145 and by the Swiss National Science Foundation Grant PP00P2_163681.

Appendix A. Supplementary material

Notes for sample preparation, *in situ* melting and vitrification, heat transfer simulations, characterization of the temperature evolution and time resolution with time-resolved EM, analysis of the time-resolved diffraction patterns, and fitting procedure for the heating and cooling times; figures for sample preparation for graphene-enclosed cryo samples, sketch of modified transmission electron microscope, heat transfer simulations, time-resolved diffraction data, time-resolved cryo-EM GroEL experiments. Supplementary data to this article can be found online at https://doi.org/10.1016/j.cplett.2021.138812.

References

[1] K. Henzler-Wildman, D. Kern, Dynamic personalities of proteins, Nature 450 (2007) 964–972.
[2] D.D. Boehr, H.J. Dyson, P.E. Wright, An NMR perspective on enzyme dynamics, Chem. Rev. 106 (2006) 3055–3079.
[3] J. Frank, Conformational Proteomics of Macromolecular Architecture: Approaching the Structure of Large Molecular Assemblies and Their Mechanisms of Action Ch. 13, World Scientific, Singapore, 2004.
[4] J. Frank, Three-Dimensional Electron Microscopy of Macromolecular Assemblies: Visualization of Biological Molecules in Their Native State, Oxford University Press, New York, 2006.
[5] E. Cao, M. Liao, Y. Cheng, D. Julius, TRPV1 structures in distinct conformations reveal activation mechanisms, Nature 504 (2013) 113–118.
[6] J. Zhao, S. Benlekbir, J.L. Rubinstein, Electron cryomicroscopy observation of rotational states in a eukaryotic V-ATPase, Nature 521 (2015) 241–245.
[7] Y. Shi, A glimpse of structural biology through x-ray crystallography, Cell 159 (2014) 995–1014.
[8] F. Schotte, M. Lim, T.A. Jackson, A.V. Smirnov, J. Soman, J.S. Olson, G.N. Jr, M. Phillips, P.A. Anfinrud Wulff, Watching a protein as it functions with 150-ps time-resolved x-ray crystallography, Science 300 (2003) 1944–1947.
[9] K. Pande, C.D.M. Hutchison, G. Groenhof, A. Aquila, J.S. Robinson, J. Tenboer, S. Basu, S. Boutet, D.P. DePonte, M. Liang, T.A. White, N.A. Zatsepin, O. Yefanov, D. Morozov, D. Oberthuer, C. Gati, G. Subramanian, D. James, Y. Zhao, J. Koralek, J. Brayshaw, C. Kupitz, C. Conrad, S. Roy-Chowdhury, J.D. Coe, M. Metz, P.L. Xavier, T.D. Grant, J.E. Koglin, G. Ketawala, R. Fromme, V. rajer, R. Henning, J.C.H. Spence, A. Ourmazd, P. Schwander, U. Weierstall, M. Frank, P. Fromme, A. Barty, H.N. Chapman, K. Moffat, J.J. van Thor, M. Schmidt, Femtosecond structural dynamics drives the trans/cis isomerization in photoactive yellow protein, Science. 352 (2016) 725–729.
[10] S. Skou, R.E. Gillilan, N. Ando, Synchrotron-based small-angle x-ray scattering of proteins in solution, Nat. Protoc. 9 (2014) 1727–1739.
[11] S.P. Meisburger, W.C. Thomas, M.B. Watkins, N. Ando, X-ray scattering studies of protein structural dynamics, Chem. Rev. 117 (2017) 7615–7672.
[12] M.C. Deller, L. Kong, B. Rupp, Protein stability: a crystallographer's perspective, Acta Cryst. F 72 (2016) 72–95.
[13] X. Li, P. Mooney, S. Zheng, C.R. Booth, M.B. Braunfeld, S. Gubbens, D.A. Agard, Y. Cheng, Electron counting and beam-induced motion correction enable near-atomic-resolution single-particle cryo-EM, Nat. Methods. 10 (2013) 584–590.
[14] W. Kuhlbrandt, The resolution revolution, Science 343 (2014) 1443–1444.
[15] R. Henderson, Overview and future of single particle electron cryomicroscopy, Arch. Biochem. Biophys. 581 (2015) 19–24.
[16] Y. Cheng, N. Grigorieff, P.A. Penczek, T. Walz, A primer to single-particle cryo-electron microscopy, Cell 161 (2015) 438–449.
[17] X. Bai, G. McMullan, S.H.W. Scheres, How cryo-EM is revolutionizing structural biology, Trends Biochem. Sci. 40 (2015) 49–57.
[18] A. Merk, A. Bartesaghi, S. Banerjee, V. Falconieri, P. Rao, M.I. Davis, R. Pragani, M. B. Boxer, L.A. Earl, J.L.S. Milne, S. Subramaniam, Breaking cryo-EM resolution barriers to facilitate drug discovery, Cell 165 (2016) 1698–1707.
[19] E. Nogales, The development of cryo-EM into a mainstream structural biology technique, Nat. Methods. 13 (2016) 24–27.
[20] M. Adrian, J. Dubochet, J. Lepault, A.W. McDowall, Cryo-electron microscopy of viruses, Nature 308 (1984) 32–36.
[21] J. Dubochet, M. Adrian, J.-J. Chang, J.-C. Homo, J. Lepault, A.W. McDowall, P. Schultz, Cryo-electron microscopy of vitrified specimens, Q. Rev. Biophys. 21 (1988) 129–228.
[22] B. Chen, J. Frank, Two promising future developments of cryo-EM: capturing short-lived states and mapping a continuum of states of a macromolecule, Microscopy. 65 (2016) 69–79.
[23] J. Frank, Time-resolved cryo-electron microscopy: Recent progress, J. Struct. Biol. 200 (2017) 303–306.
[24] Z. Lu, T.R. Shaikh, D. Barnard, X. Meng, H. Mohamed, A. Yassin, C.A. Mannella, R. K. Agrawal, T.-M. Lu, T. Wagenknecht, Monolithic microfluidic mixing–spraying devices for time-resolved cryo-electron microscopy, J. Struct. Biol. 168 (2009) 388–395.
[25] T.R. Shaikh, A.S. Yassin, Z. Lu, D. Barnard, X. Meng, T.-M. Lu, T. Wagenknecht, R. K. Agrawal, Initial bridges between two ribosomal subunits are formed within 9.4 milliseconds, as studied by time-resolved cryo-EM, Proc. Natl. Acad. Sci. 111 (2014) 9822–9827.
[26] V.P. Dandey, W.C. Budell, H. Wei, D. Bobe, K. Maruthi, M. Kopylov, E.T. Eng, P. A. Kahn, J.E. Hinshaw, N. Kundu, C.M. Nimigean, C. Fan, N. Sukomon, S.A. Darst, R.M. Saecker, J. Chen, B. Malone, C.S. Potter, B. Carragher, Time-resolved cryo-EM using Spotiton, Nat. Methods. 17 (2020) 897–900.
[27] J.F. Menetret, W. Hofmann, R.R. Schroder, G. Rapp, R.S. Goody, Time-resolved cryo-electron microscopic study of the dissociation of actomyosin induced by photolysis of photolabile nucleotides, J. Mol. Biol. 219 (1991) 139–144.
[28] T.R. Shaikh, D. Barnard, X. Meng, T. Wagenknecht, Implementation of a flash-photolysis system for time-resolved cryo-electron microscopy, J. Struct. Biol. 165 (2009) 184–189.
[29] G.C.R. Ellis-Davies, Caged compounds: photorelease technology for control of cellular chemistry and physiology, Nat. Methods. 4 (2007) 619–628.
[30] Y. Shigeri, Y. Tatsu, N. Yumoto, Synthesis and application of caged peptides and proteins, Pharmacol. Ther. 91 (2001) 85–92.
[31] C.J. Russo, L.A. Passmore, Ultrastable gold substrates for electron cryomicroscopy, Science 346 (2014) 1377–1380.
[32] J.M. Yuk, J. Park, P. Ercius, K. Kim, D.J. Hellebusch, M.F. Crommie, J.Y. Lee, A. Zettl, A.P. Alivisatos, High-resolution EM of colloidal nanocrystal growth using graphene liquid cells, Science 336 (2012) 61–64.
[33] P.K. Olshin, M. Drabbels, U.J. Lorenz, Characterization of a time-resolved electron microscope with a Schottky field emission gun, Struct. Dyn. 7 (2020), 054304.
[34] A.H. Zewail, Four-dimensional electron microscopy, Science 328 (2010) 187–193.

[35] U.J. Lorenz, A.H. Zewail, Observing liquid flow in nanotubes by 4D electron microscopy, Science 344 (2014) 1496–1500.
[36] R.J.D. Miller, Femtosecond crystallography with ultrabright electrons and x-rays: capturing chemistry in action, Science 343 (2014) 1108–1116.
[37] A. Feist, K.E. Echternkamp, J. Schauss, S.V. Yalunin, S. Schäfer, C. Ropers, Quantum coherent optical phase modulation in an ultrafast transmission electron microscope, Nature 521 (2015) 200–203.
[38] S.K. Sinha, A. Khammari, M. Picher, F. Roulland, N. Viart, T. LaGrange, F. Banhart, Nanosecond electron pulses in the analytical electron microscopy of a fast irreversible chemical reaction, Nat. Commun. 10 (2019) 3648.
[39] B.E. Warren, X-Ray Diffraction, Dover Publications, New York, 1990.
[40] P. Jenniskens, D.F. Blake, Structural transitions in amorphous water ice and astrophysical implications, Science 265 (1994) 753–756.
[41] P. Brüggeller, E. Mayer, Complete vitrification in pure liquid water and dilute aqueous solutions, Nature 288 (1980) 569–571.
[42] M.J. Dobro, L.A. Melanson, G.J. Jensen, A.W. McDowall, Methods in Enzymology Ch. 3, Elsevier, London, 2010.
[43] J.A. McMillan, S.C. Los, Vitreous ice: irreversible transformations during warm-up, Nature 206 (1965) 806–807.
[44] G.P. Johari, A. Hallbrucker, E. Mayer, The glass–liquid transition of hyperquenched water, Nature 330 (1987) 552–553.
[45] S. Chen, A.M. Roseman, A.S. Hunter, S.P. Wood, S.G. Burston, N.A. Ranson, A. R. Clarke, H.R. Saibil, Location of a folding protein and shape changes in GroEL–GroES complexes imaged by cryo-electron microscopy, Nature 371 (1994) 261–264.
[46] R.M. Glaeser, K.A. Taylor, Radiation damage relative to transmission electron microscopy of biological specimens at low temperature: a review, J. Microsc. 112 (1978) 127–138.
[47] R.M. Glaeser, Methods in Enzymology Ch. 2, Elsevier, London, 2016.
[48] S. Uehara, H. Nikjoo, Monte Carlo Simulation of Water Radiolysis for Low-energy Charged Particles, J. Radiat. Res. (Tokyo) 47 (2006) 69–81.
[49] R.J.D. Miller, O. Paré-Labrosse, A. Sarracini, J.E. Besaw, Three-dimensional view of ultrafast dynamics in photoexcited bacteriorhodopsin in the multiphoton regime and biological relevance, Nat. Commun. 11 (2020) 1240.
[50] M. Gutman, Methods of Biochemical Analysis Ch. 1, John Wiley & Sons, Inc., New York, 1984.